J Appl Electrochem (2008) 38:1159–1170
DOI 10.1007/s10800-008-9548-9

ORIGINAL PAPER

Electrochemical promotion of NO reduction by C_2H_4 in 10% O_2 using a monolithic electropromoted reactor with Rh/YSZ/Pt elements

S. Souentie · A. Hammad · S. Brosda · G. Foti · C. G. Vayenas

Received: 29 October 2007 / Revised: 5 March 2008 / Accepted: 7 March 2008 / Published online: 26 March 2008

Abstract The reduction of NO by C_2H_4 in high excess of O_2 and temperatures 200−300 °C was investigated using a monolithic electropromoted reactor (MEPR) with twenty-two Rh/YSZ/Pt parallel plate elements. It was found that at 220–240 °C and 10% O_2 the selective catalytic reduction (SCR) of NO can be electropromoted by 450% with near 100% selectivity to N_2 and Λ_{NO} values up to 2.4. The corresponding rate enhancement ratio of complete C_2H_4 oxidation is up to 900% with Faradaic efficiency, Λ_{CO_2}, values up to 350. The system appears promising for practical applications.

Keywords Electrochemical promotion · NEMCA effect · NO reduction · Ethylene reductant · Monolithic electropromoted reactor · Selective catalytic reduction (SCR) of NO · Rhodium electrocatalyst · Platinum electrocatalyst

1 Introduction

The reduction of NO by light hydrocarbons in the presence of 10% O_2, typical of the exhaust of lean-burn and Diesel engines, presents a great technological challenge [1–7]. Although Cu-ZSM5 type catalysts show good activity and selectivity, their overall thermal stability and performance is not sufficient to lead to a commercial process [8, 9]. Noble metals (Rh, Pt and Pd) exhibit good activity for NO reduction, but are poisoned severely by strong adsorption of oxygen for p_{O_2} values exceeding 2% [1–7]. This is particularly pronounced for Rh, which exhibits high selectivity to N_2 and is less pronounced for Pt, which however exhibits lower selectivity to N_2, and significant N_2O formation at lower temperatures.

Many previous studies with supported catalysts have focused on the use of simulated exhaust gas mixtures containing HC/NO/O_2 concentrations in the range 1,000 ppm/1,000 ppm/5% and H_2, CH_4, C_2H_4 or C_3H_6 reductant over dispersed catalysts in fixed bed or fluidized bed reactors [1–15].

Few studies have investigated the high O_2 excess (∼10%) range which is of significant practical importance. Chen et al. [14] reported 70% NO conversion using CO as a reductant over Pd/$CeZrO_2$ with 85% N_2 selectivity at 400 °C and Wang et al. [15] found 85% NO conversion to N_2 using as reductant C_2H_2 over Ce-zeolites at 300 °C.

A parallel approach has been the use of the electrochemical promotion of catalysis (EPOC or NEMCA effect [15–23] to electropromote Pt, Rh and Pd catalysts [23–51], (Appendix 1), in some case in conjunction with classical (chemical) promotion [32]. These studies have utilized YSZ [24–39], β''-Al_2O_3 [40–49], Nasicon [50], and proton conductor [51] solid electrolytes and, with very few recent exceptions [34–38], thick (0.5–1 μm) porous metal films. With a very recent exception utilizing Pt–Rh alloy catalysts [38], they were also limited to p_{O_2} values below 2% where the O_2 poisoning problem is not pronounced. The large majority of these studies were also limited to single-pellet reactors and only recently a monolithic electropromoted reactor (MEPR) was utilized for laboratory studies [34–38] and also tested under real car exhaust conditions [37] with

S. Souentie · A. Hammad · S. Brosda · C. G. Vayenas (✉)
Department of Chemical Engineering, University of Patras, Caratheodory 1 St., 26504 Patras, Greece
e-mail: cat@chemeng.upatras.gr

G. Foti
Institute of Chemical Sciences and Engineering, Ecole Polytechnique Fédérale de Lausanne, 1015 Lausanne, Switzerland

moderate success and under relatively high fuel injection in the exhaust.

The present study is the first one utilizing hydrocarbon, NO and O_2 concentrations typical of real Diesel exhaust conditions (1,000 ppm hydrocarbon, 660 ppm NO, 10% O_2) and low enough temperatures (down to 200 °C). Similar to previous works [34, 37], we have used Rh/YSZ/Pt catalyst elements in an effort to utilize simultaneously the advantages of both Rh and Pt, i.e. strong electropromotion of Rh with anodic potential [29–37] and of Pt with cathodic potential [28, 41–45], high selectivity to N_2 on Rh [1–10], lower susceptibility to O_2 on Pt and, perhaps, ability of Rh to dissociate N_2O formed on Pt.

Two parameters are commonly used to describe the magnitude of electrochemical promotion, i.e. the Faradaic efficiency, Λ, and the rate enhancement ratio, ρ [19–23]. In the present case of NO reduction by C_2H_4 in presence of O_2 they are defined from:

$$\Lambda_{CO_2} = \Delta r_{CO_2}/(I/2F); \quad \Lambda_{NO} = \Delta r_{NO}/(I/2F)$$

$$\rho_{CO_2} = (r_{o,CO_2} + \Delta r_{CO_2})/r_{o,CO_2}; \quad \rho_{NO} = (r_{o,NO} + \Delta r_{NO})/r_{o,NO} \tag{1}$$

where r_{CO_2} and r_{NO} (the total rate of consumption of NO) are expressed in mol O and subscript "o" denotes open-circuit conditions. In addition to these parameters, when describing electropromotion at high reactant conversions, as in the present case, it is important to define a third parameter, the effective rate enhancement ratio, ρ_c, defined from:

$$\rho_c = \rho/\rho_{max} \tag{2}$$

where ρ_{max} expresses the maximum allowable ρ value due to complete or, more generally, equilibrium conversion.

It should be noted that, in the present study, both the Rh and Pt films are catalytically active and therefore the measured r_{CO_2} and r_{N_2} values correspond to the sum of the rates on the Rh and Pt catalyst films. Therefore the terms "electrophobic" ($\partial r/\partial U > 0$) "electrophilic" ($\partial r/\partial U < 0$), "volcano" and "inverted volcano" [23] used to describe the observed electropromotion behaviour are used in a broad sense, characterizing the electropromotion behaviour of the Rh/YSZ/Pt elements (U is the potential of the Rh catalyst-electrode relative to the Pt electrode) rather than that of the individual Rh and Pt catalysts.

2 Experimental

2.1 YSZ solid electrolyte plates

The solid electrolyte plates provided by Bosch had a thickness of 0.25 mm and dimensions of 50 mm × 50 mm. They were made of yttria-stabilized zirconia (YSZ, 8 wt.% Y_2O_3 with a resulting molar composition $Zr_{0.913}Y_{0.087}O_{1.957}$). The starting material had a mean particle size of 0.5 μm. The density in the sintered state was between 5.7 and 5.9 g cm^{-3}.

2.2 Sputter deposition and characterization of the Rh and Pt catalyst films

The Rh/YSZ/Pt and Rh/YSZ/Au samples were prepared by metal sputtering. Prior to Rh, Pt or Au deposition, no surface treatment was performed. The YSZ support was introduced into the sputtering chamber, filled with pure argon, then metal (Rh 99.8 or Pt 99.99, Lesker) was deposited onto the substrate at 50 °C. The sputtering conditions were the following: direct current (dc) mode with a discharge of 350 V, argon pressure of 0.5 Pa. Under these conditions the deposition rate is 0.10–0.15 nm s^{-1}. The film thickness was measured by calibration with smooth silicon samples processed simultaneously [34]. The thickness of the sputter-deposited rhodium and platinum films was approximately 40 nm.

The surface area of the Rh and Pt catalyst films, as well as the metal dispersion, was estimated using the galvanostatic transient technique, by measuring the time constant, τ, required for the rate increase, Δr, in galvanostatic electropromotion rate transients to reach 63% of its steady-state value [23]. In this way one can estimate the reactive oxygen uptake, N_G, of the anodically polarized metal film and, assuming a 1:1 surface metal:O ratio, the active catalyst surface area, N_G, expressed in mol, calculated by:

$$N_G = \frac{I\tau}{2F} \tag{4}$$

during the current imposition [23] or by:

$$N_G = \frac{r\tau_D}{\Lambda} \tag{5}$$

in the current interruption technique [23], where r is the electropromoted rate and the depolarization time, τ_D, expresses the average lifetime of the backspillover oxygen species originating from the YSZ lattice. These promoting $O^{\delta-}$ species are more strongly bonded to the catalytic surface than normally adsorbed oxygen [23].

These experiments were conducted both with anodic and cathodic polarization in an effort to estimate the surface area of both the Rh and Pt catalysts (Table 1).

As in a previous study [34], the total surface area of the Rh catalysts per plate was estimated to be (1.3–5.6) × 10^{-6} mol Rh and (1.8–4.3) × 10^{-6} mol Pt. Since the metal loading per plate is of the order of 10^{-5} mol Rh or Pt, it follows that these thin (~40 nm) films are porous and mostly amorphous and that the Rh and Pt metal dispersions are of the order of 10−40%, i.e. comparable to that of commercial dispersed catalysts.

Table 1 N_G values estimated by current imposition (N_G-63%) and current interruption (N_G-c.i) during both positive and negative polarization under (a) 7% and (b) 9.4% oxygen excess

T (°C)	N_G-63% positive 22 plates/mol Rh	N_G-c.i. positive 22 plates/mol Rh	N_G-c.i. positive per plate/mol Rh	N_G-63% negative 22 plates/mol Pt	N_G-c.i. negative 22 plates/mol Pt	N_G-c.i. negative per plate/mol Pt
(a)						
240	6.50×10^{-5}	2.88×10^{-5}	1.3×10^{-6}	8.56×10^{-5}	9.50×10^{-5}	4.3×10^{-6}
(b)						
240	6.06×10^{-6}	1.23×10^{-4}	5.6×10^{-6}	8.16×10^{-6}	4.03×10^{-5}	1.8×10^{-6}

2.3 MEP reactor operation

The MEP reactor was placed in a tubular furnace and its temperature was measured and controlled by a type K thermocouple at a distance of 1 mm from the gas entrance. A significant improvement in the design of the MEP reactor used here in relation to previous ones [34–37] was the use of gas-tight vacuum feed-throughs for the introduction of the two wires connected to the reactor elements. This has significantly improved the gas-tightness of the reactor which is an important consideration since the reduction of NO is quite sensitive to the oxygen partial pressure. The feed gas composition and total flow rate, F_T, was controlled by four mass flowmeters (Brooks smart mass flow and controller B5878). Reactants were Messer–Griesheim certified standards of C_2H_4 in He, O_2 in He and NO in He. Pure He (99.99%) was fed through the fourth flowmeter in order to further adjust total flow rate and inlet gas composition at desired levels. In all experiments discussed here the total inlet volumetric flow rate, F_T, was maintained at 1 dm^3 STP min^{-1}. Reactants and products were analyzed by on-line gas chromatography (Varian 3800 equipped with a Porapak Q column at 50 °C for the separation of C_2H_4, CO_2 and N_2O and a Molecular Sieve column at 70 °C for the separation of N_2 and O_2), in conjunction with an IR CO–CO_2 analyzer (Fuji Electric) and a chemiluminescence (ECO Physics CLD 700 EL ht) NO/NOx analyzer. Constant currents and potentials were applied using an AMEL 2053 galvanostat-potentiostat.

A parameter frequently used in automotive catalysis is the lambda (λ) factor. This factor is used to describe the O_2/fuel ratio present in an automotive exhaust and is defined from:

$$\lambda = \frac{\text{actual (air/fuel) ratio}}{\text{stoichiometric (air/fuel) ratio}} \tag{6}$$

and in the case of C_2H_4 as fuel, is calculated by:

$$\lambda = \frac{1}{3}\frac{y^{in}_{O_2} + \frac{y^{in}_{NO}}{2}}{y^{in}_{C_2H_4}} \tag{7}$$

while, the O_2 excess (Π) is defined from:

$$\Pi = \left(y_{O_2} + \frac{y_{NO}}{2}\right) - 3y_{C_2H_4} \tag{8}$$

In a conventional spark-ignition engine exhaust, λ is close to unity, while in lean burn engines, where Π is about 10%, λ can be up to 17.

3 Results and discussion

The experiments were performed using three gaseous feed compositions:

a. Near stoichiometric oxygen conditions, i.e. $p_{C_2H_4} = 0.36$ kPa, $P_{NO} = 0.11$ kPa, $p_{O_2} = 1.1$ kPa, thus $\lambda = 1.12$, $\Pi = 0.08\%$.
b. Medium oxidizing conditions, i.e. $p_{C_2H_4} = 1$ kPa, $P_{NO} = 0.066$ kPa, $p_{O_2} = 10$ kPa, thus $\lambda = 3.3$, $\Pi = 7.03\%$.
c. Highly oxidizing conditions, i.e. $p_{C_2H_4} = 0.2$ kPa, $P_{NO} = 0.066$ kPa, $p_{O_2} = 10$ kPa, thus $\lambda = 16.7$, $\Pi = 9.43\%$.

3.1 Near stoichiometric oxygen conditions ($\lambda = 1.12$)

Figure 1 shows anodic galvanostatic transient obtained in a slightly oxidizing C_2H_4–NO–O_2 mixture, where Π is 0.08% and λ is 1.12. Upon positive current imposition (+30 mA) the ethylene conversion increases from 26% to 78% ($\rho_{CO_2} = 2.8$), O_2 conversion increases from 29% to 83%, while the NO conversion increases from 28% to 94%($\rho_{NO} = 3.37$). Furthermore, the effective enhancement ratio, ρ_c, for the CO_2 production rate is 0.78, while for the NO reduction rate it reaches 0.94, which means that the achieved NO conversion via the NEMCA effect is 94% of the maximum possible conversion (100%). No measurable concentration of N_2O was found in the products and thus N_2 was the only measurable product of the reduction of NO. Also no measurable concentration of NO_2 was detected. The observed high selectivity to N_2 implies that all N_2O possibly produced by NO reduction on the Pt catalyst-electrodes is further reduced to N_2 on the Rh

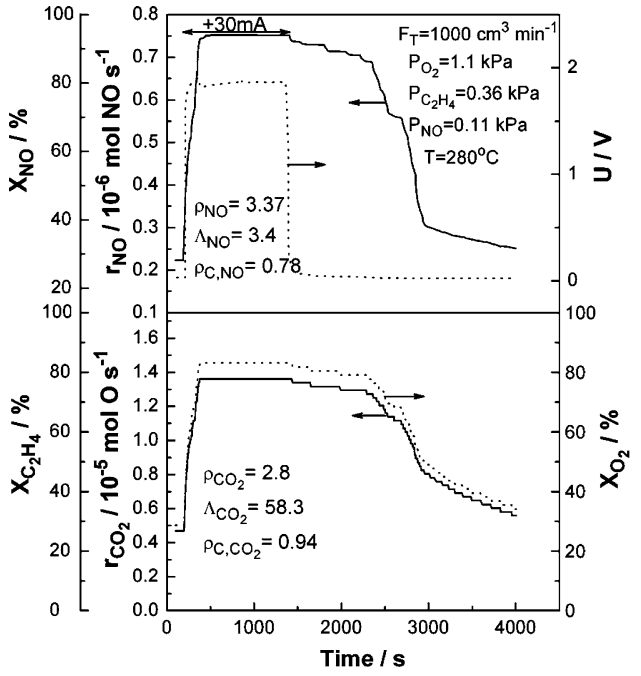

Fig. 1 Transient effect of a constant applied current (+30 mA) on the catalytic rate of NO reduction (r_{NO}) and CO_2 formation (r_{CO_2}), on the NO, C_2H_4 and O_2 conversion (X_{NO}, $X_{C_2H_4}$, X_{O_2}) and on the Rh–Pt potential difference (U). T = 280 °C

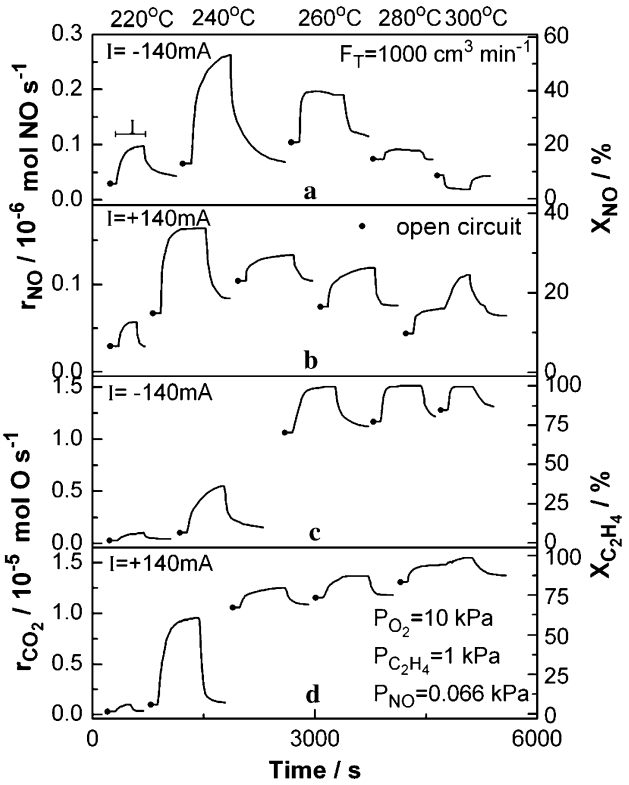

Fig. 2 Transient responses at five different temperatures of NO conversion and CO_2 formation rates and of the conversion of NO and C_2H_4 upon constant negative (**a**, **c**) and positive (**b**, **d**) current imposition. $O_2/C_2H_4/NO$ = 10 kPa/1 kPa/0.066 kPa

catalyst-electrodes [23, 25, 26]. The phenomenon is reversible, since current interruption causes both rates to return to their initial values after approximately 70 min (Fig. 1).

It is worth noting in Fig. 1 and subsequent figures that $|\Lambda_{NO}|$ is much smaller than $|\Lambda_{CO_2}|$, typically by a factor of 20–100. This is because, as in all previous studies of NO reduction on Rh or Pt metal catalysts, the rate of NO reduction, particularly under oxidizing conditions, is typically a factor of 20–100 smaller than the rate of hydrocarbon oxidation. This reflects the fact that the rate of NO reduction is intrinsically much slower than the rate of hydrocarbon oxidation on these surfaces. Typical turnover frequencies (TOFs) for NO reduction are 10^{-3} s^{-1} vs 10^{-1} s^{-1} for hydrocarbon oxidation [23]. Thus, since the order of magnitude of $|\Lambda|$ can be estimated from [23]:

$$|\Lambda| = 2Fr_o/I_o \quad (9)$$

where I_o is the exchange current of the catalyst/electrode in presence of the reacting mixture, one can rationalize immediately the observed large $|\Lambda_{CO_2}/\Lambda_{NO}|$ ratios.

The observed (Fig. 2) overall electrophobic behaviour, i.e. rate increase with potential, is similar to that obtained in previous electropromotion studies of NO reduction on Rh [23, 29–32] and can be rationalized by accounting for the effect of decreasing strength of oxygen chemisorption on Rh with anodic polarization due to the repulsive lateral interactions with the spillover O^{2-} species. On the other hand the NO reduction on Pt under near stoichiometric oxygen conditions is known [23, 28] to exhibit electrophilic behaviour, due to weaker oxygen chemisorption [23, 28] so that the effect seen in Fig. 1 and subsequent figures is the sum of the electropromotion effect of Rh (anodic polarization) and Pt (cathodic polarization). These two effects cannot be, unfortunately, separated in a MEPR with Rh/YSZ/Pt elements. Such a separation requires the use of more-or-less inert (e.g. Au) counter electrodes as is done in single chamber studies of the electropromotion of NO reduction [24–33, 41–51].

3.2 Medium oxidizing conditions (λ = 3.3)

Figure 2 shows five galvanostatic transient responses of the NO reduction rate (a, b) and of the CO_2 production rate (c, d) upon application of constant anodic (b, d) and cathodic (a, c) current at temperatures 220, 240, 260, 280 and 300 °C, using 1 kPa C_2H_4, 10 kPa O_2, and 0.066 kPa NO and total gas flowrate 1,000 cm^3 min^{-1}. Again no measurable concentration of N_2O was detected and, at 240 °C or below, no measurable concentration of NO_2 was found in the products as shown below. One observes in Fig. 2 that the open-circuit C_2H_4 conversion increases from

2% to 82.1% as temperature is increased from 220 to 300 °C. The open-circuit NO conversion, however, increases from 4.5% to 21% between 220 and 260 °C, where it exhibits a maximum and then decreases significantly. Both positive and negative currents cause a very pronounced and reversible increase in both r_{CO_2} and r_{NO}. The electrochemical promotion effect is maximum at 240 °C.

Thus, at 240 °C and under negative polarization (−3.5 V) the NO conversion increases from 13.5% to 53% while the C_2H_4 conversion increases from 6.3% to 62%. One also observes the decreasing electropromotion effect with increasing temperature and the purely electrophobic nature of the reduction of NO at 300 °C. At lower temperatures both rates are enhanced both with positive and negative potential.

The above maximum electropromotion effect on both CO_2 formation and NO reduction, expressed in terms of average TOFs and conversions, is depicted more clearly in Fig. 3. Upon imposing a cathodic current −140 mA, the C_2H_4 conversion increases from 6.3% to 36.5% ($\rho_{CO_2} = 5.8$), the NO conversion increases from 13.6% to 53.1% ($\rho_{NO} = 3.9$) while the O_2 conversion increases from 4% to 11%. The developed potential is approximately −4.5 V due to the low operating temperature. The corresponding Λ_{CO_2} and Λ_{NO}, are 18.6 and 0.3, respectively.

Figure 4 shows the steady-state effect of the applied anodic and cathodic current on the NO reduction rate, on the CO_2, CO and NO_2 production rates as well as on the conversion of both reactants as a function of temperature. There is an increase in the rate of NO consumption with both positive and negative current, with a maximum effect at 240 °C upon cathodic polarization. Normally in the electrochemical promotion literature such behaviour (i.e. rate increase with both positive and negative current or, equivalently, existence of a minimum in the rate vs potential curve) is termed inverted volcano behaviour [23]. We will use this term here too, although in the present case it is only a phenomenologic definition, since the Pt counter electrode is also catalytically active. As shown in Fig. 4, inverted volcano behaviour is also noted in the CO_2 production, in the temperature range 220–300 °C. NO_2 production starts to take place with cathodic polarization above the ignition temperature of the catalyst (∼240 °C) which also coincides with the disappearance of CO produced in small amounts at lower temperatures and cathodic polarization. At higher temperatures (260 and 280 °C) there is significant production of NO_2 with cathodic polarization.

Figure 5 depicts the steady state effect of temperature on the rate enhancement, ρ, and on the Faradaic efficiency, Λ, for NO reduction and CO_2 production. ρ_{CO_2} and Λ_{CO_2} go through a maximum in the temperature range 230–250 °C, reaching 10 and 36, respectively, while similar is the behaviour of ρ_{NO} and Λ_{NO}. The subsequent increase in ρ_{NO} at higher temperatures is due to the formation of NO_2.

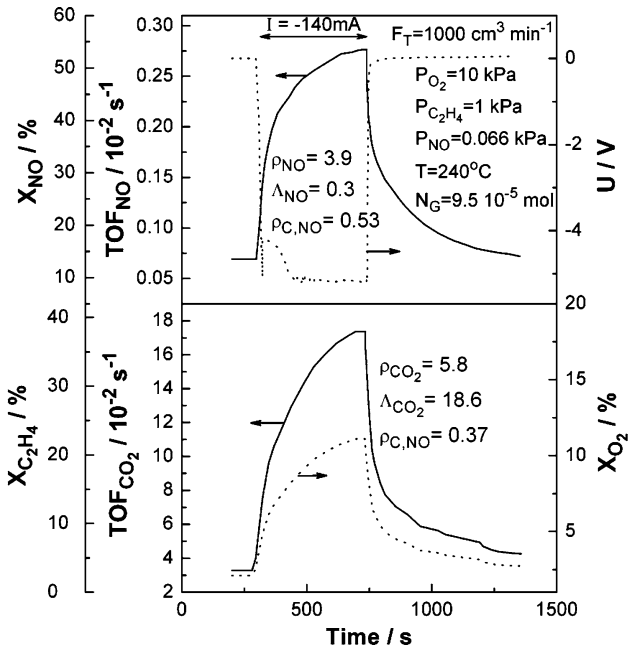

Fig. 3 Transient effect of a constant applied negative current (−140 mA) on the catalytic rates of NO conversion (r_{NO}) and CO_2 formation (r_{CO_2}), on the NO, C_2H_4 and O_2 conversion (X_{NO}, $X_{C_2H_4}$, X_{O_2}) and on the Rh–Pt potential difference (U). T = 240 °C

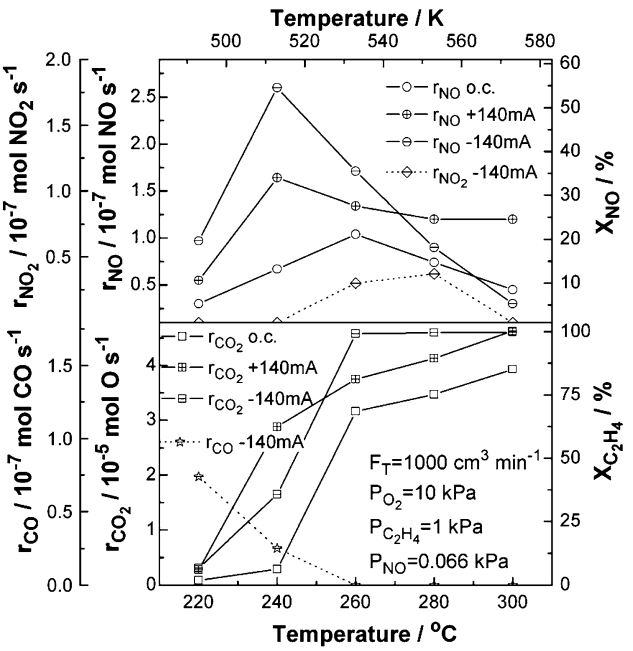

Fig. 4 Steady state effect of temperature on the NO conversion rate, on the CO_2, CO and NO_2 production rates and on the conversion of C_2H_4 and NO, under open and closed circuit conditions

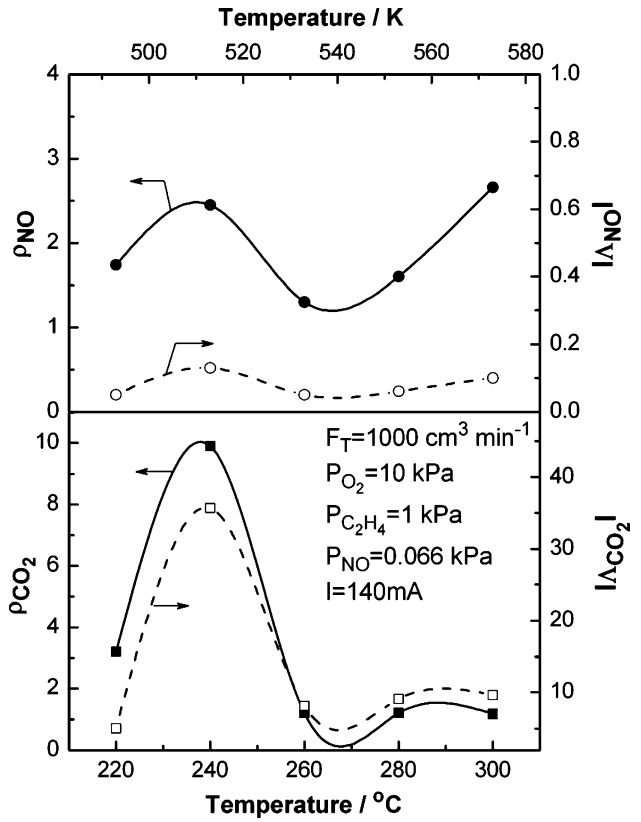

Fig. 5 Steady state effect of temperature on the rate enhancement ratio and on the apparent Faradaic efficiency of both the NO conversion and CO_2 formation reactions at medium oxidizing conditions

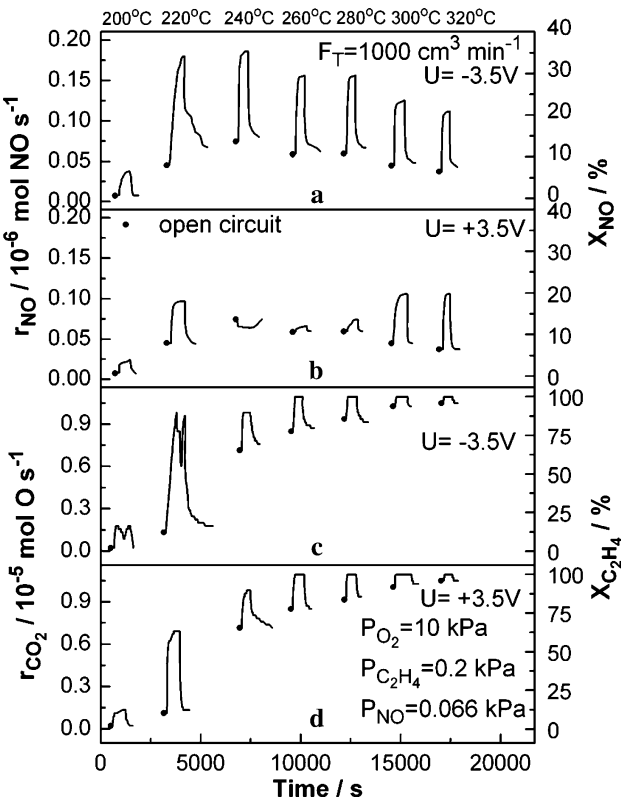

Fig. 6 Transient responses at five different temperatures of the NO conversion and CO_2 formation rates and of the conversion of NO and C_2H_4 upon constant negative (**a**, **c**) and positive (**b**, **d**) current imposition. $O_2/C_2H_4/NO$ = 10 kPa/0.2 kPa/0.066 kPa

3.3 Highly oxidizing conditions ($\lambda = 16.7$)

In order to simulate the actual conditions of the exhaust of a lean burn engine, similar experiments were performed by feeding the reactor with a mixture of 0.2 kPa C_2H_4, 10 kPa O_2 and 0.066 kPa NO balanced in He, thus $\lambda = 16.7$ and $\Pi = 9.43\%$.

Figure 6 shows anodic galvanostatic transient responses of the NO consumption rate (a, b) and the CO_2 production rate (c, d) upon application of constant anodic (b, d) and cathodic (a, c) current, in the temperature range of 220–300 °C and total gas flowrate 1,000 cm^3 min^{-1}. Similar behaviour with the case of 7% oxygen excess, Fig. 2, is noted, with relatively minor differences. Similarly to the $\lambda = 3.3$ case, there is no N_2O production and also under open-circuit practically no NO_2 production. However at 240 °C and higher temperatures there is significant production of NO_2 with cathodic polarization as discussed below. As shown in Fig. 6 the C_2H_4 conversion increases with temperature from 2.5% to 92%. The NO conversion under open circuit state increases from 1.5% at 200 °C to 17% at ~240 °C where a maximum appears. Under polarization conditions the NO conversion exhibits the same behaviour, both with positive and negative potential application, except for the case at the intermediate temperature of 240 °C, where it exhibits a weak electrophilic behaviour. The same change in behaviour, but at higher temperatures, was observed in the medium oxygen excess case.

Figure 7 shows potentiostatic transients at the optimal operating temperature of 220 °C where upon negative potential application the conversion of NO increases from 8% to 35% with a Λ_{NO} value of 2.35.

Interestingly, upon negative potential interruption, r_{NO} decreases in small successive steps, while r_{CO_2} exhibits a more complex transient, first decreasing, then passing through a sharp maximum. The observed steps may be related to the slightly different performance of different plates. The transient rate maximum upon potential interruption, coupled with the observed transient rate maximum upon potential imposition, may reflect the onset of site blocking effects by backspillover $O^{\delta-}$ ions on the positively polarized Pt catalyst and thus the existence of an optimal applied potential. These effects are worth further investigation, probably using inert counterelectrodes in an effort to separate the catalytic and EPOC behaviour of Rh and Pt in the MEPR environment.

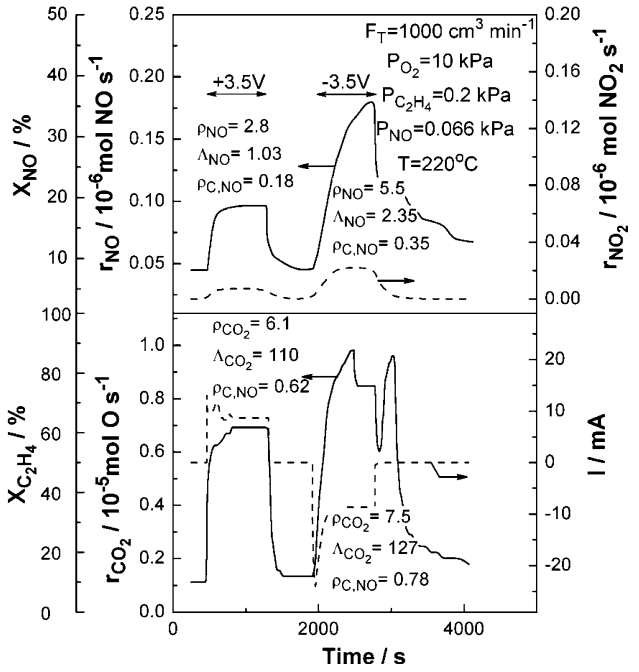

Fig. 7 Transient effect of a constant applied negative and positive potential (±3.5 V) on the rate of NO conversion (r_{NO}) and CO_2 formation (r_{CO_2}), on the NO, C_2H_4 and O_2 conversions (X_{NO}, $X_{C_2H_4}$, X_{O_2}) and on the current (I). T = 240 °C.

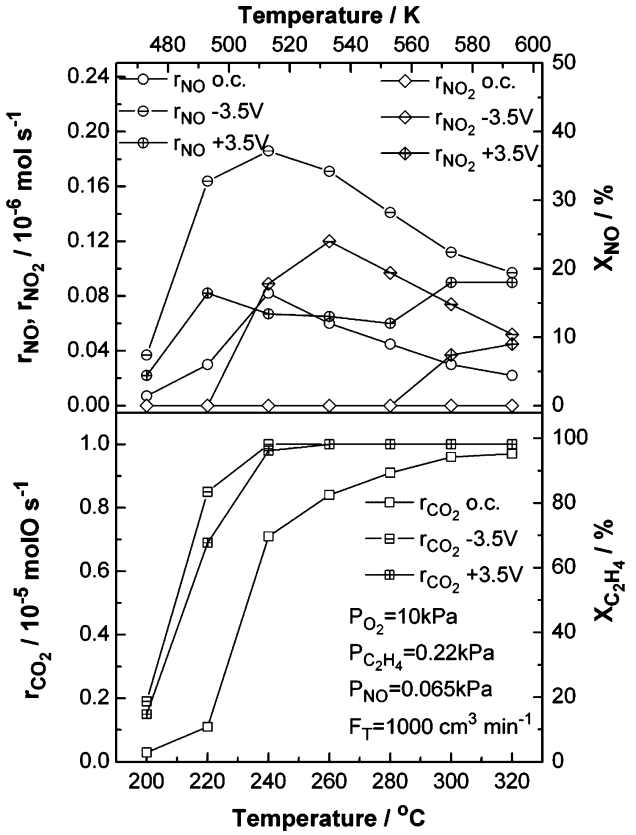

Fig. 8 Steady state effect of temperature on the NO conversion and CO_2 and NO_2 formation rates and on the conversion of C_2H_4 and NO, under open and closed circuit in highly oxidizing conditions

The magnitude of electrochemical promotion can be assessed from Fig. 8 which shows the steady state effect of temperature on the NO consumption and NO_2 formation rates (a) and on the CO_2 formation rate (b) on the Rh/YSZ/Pt electrocatalytic elements under open circuit and anodic (+3.5 V) and cathodic (−3.5 V) polarization conditions. The operating temperature ranges from 200 to 320 °C. The maximum NO conversion achieved was 37% at quite low temperatures (∼240 °C), and negative polarization corresponding to near complete C_2H_4 conversion.

The most important feature, however, of Fig. 8 has to do with the rate of NO_2 formation, r_{NO_2}, in relation to the rate of NO consumption, r_{NO}, and thus with the selectivity to N_2 defined, in absence of N_2O, as $S_{N_2} = (r_{NO} - r_{NO_2})/r_{NO}$. Thus in Fig. 8 under open-circuit it is $S_{N_2} \approx 1$ over the entire temperature range investigated. Cathodic polarization (U = −3.5 V) leads to very significant increase in r_{NO} but, at the same time, it also leads at 240 °C and above to a significant increase in r_{NO_2}, thus causing a significant decrease in S_{N_2} to values of 0.5 or less.

On the other hand, anodic polarization (U = 3.5 V) causes a smaller increase in r_{NO} but does not cause NO_2 formation below 300 °C, thus maintaining $S_{N_2} \approx 1$ over a much wider temperature range.

Thus T = 220 °C is the only temperature where the electropromotion is quite significant (Fig. 7) and at the same time the selectivity to N_2 (S_{N_2}) remains very near 100%. Such an asymmetry in the behaviour of Rh/YSZ/Pt elements regarding r_{NO_2} upon anodic and cathodic polarization has been already observed in absence of O_2 or hydrocarbons [34], albeit in the opposite direction. The difference is most likely due to the very highly oxidizing conditions in the present case. Figure 8 shows that both anodic and cathodic polarization decrease the ignition temperature by at least 20 °C (from 225 to 205 °C) and that the electropromotion of CO_2 formation is quite pronounced in this temperature range. At higher temperatures ρ_{CO_2} decreases but ρ_{c,CO_2} is near 100%, as complete C_2H_4 conversion is reached via electropromotion.

On the other hand, the electropromotion of the NO reduction obtained by negative potentials remains quite pronounced over the entire temperature range (Fig. 8, top) while positive potentials cause a 20 °C decrease (from 240 to 220 °C) in the temperature of maximum rate of NO reduction. The rate maximum in r_{NO} at these low temperatures is due to the reaction kinetics and is predicted by any type of Langmuir–Hinshelwood kinetics. The shift of the rate maximum to lower temperatures reflects the change in the binding energies of chemisorbed reactants and intermediates with potential [23].

Figure 9 shows the steady state effect of temperature on the ρ and Λ values for CO_2 production and NO

consumption, under both anodic (Fig. 9a) and cathodic (Fig. 9b) polarization. One observes that both with anodic and cathodic polarization ρ_{NO}, $|\Lambda_{NO}|$, ρ_{CO_2} and $|\Lambda_{CO_2}|$ exhibit a maximum at 220 °C. The measured maximum $|\Lambda_{NO}|$ values (1.03 and 2.35) are typically a factor of 50–100 smaller than the maximum $|\Lambda_{CO_2}|$ values, as expected from the expression $|\Lambda| \approx 2Fr_o/I_o$ [23] and the much smaller (again by a factor of 50–100) r_o values of NO reduction vs C_2H_4 oxidation (e.g. Figs. 2–6).

Figure 10 shows the steady state effect of the applied potential on the NO reduction rate, on the CO_2 formation rate and on the conversion of C_2H_4 and NO at the optimum operation temperature of 220 °C, where the maximum NO conversion was achieved. In this figure one can clearly see the inverted volcano type behaviour of the Rh/YSZ/Pt elements, i.e. the increase of the catalytic rates by both positive and negative potential application. However, the negative imposed potential branch is more effective than the positive one, as we already noticed from the previous figures. Although a maximum appears in the electropromoted rate of CO_2 formation rate and thus in C_2H_4 conversion, during negative potential imposition at −3 V, the NO reduction rate increases monotonically with decreasing potential. This is in agreement with the observation of a transient maximum in the CO_2 production rate after current interruption in Fig. 7, which as we already noted, may be due to the high coverage of $O^{\delta-}$ promoter species that is obtained on the Pt counterelectrode at such high values of negative applied potentials. As already discussed, it will be necessary to use inert counterelectrodes in a MEPR environment in order to investigate this phenomenon thoroughly. On the other hand, a monotonic increase in both rates is observed for the positive potential branch.

Figure 11 shows the corresponding effect of the applied potential on the rate enhancement ratio (ρ) and Faradaic efficiency (Λ) for the CO_2 formation and NO reduction catalytic rates at the optimum operation temperature of 220 °C. The figure also shows the corresponding effective rate enhancement ratios ρ_c. Similar behaviour to the one of Fig. 10 is observed. The rate enhancement ratio for the CO_2 formation reaction goes through a maximum at ~3 V in correspondence to the maximum in the CO_2 formation rate (Fig. 10). The measured, ρ values vary from 1.2 to 10 for the CO_2 formation rate and from 1.1 to 5.6 for the NO reduction rate, while maximum absolute Λ values are of the order of 2 for NO reduction and of 200 for CO_2 formation. The corresponding effective rate enhancement ratios, ρ_c, approach 0.45 for NO conversion and one for CO_2 production with negative polarization. These high values show the very good performance of the MEP reactor at the optimal temperature of 220 °C.

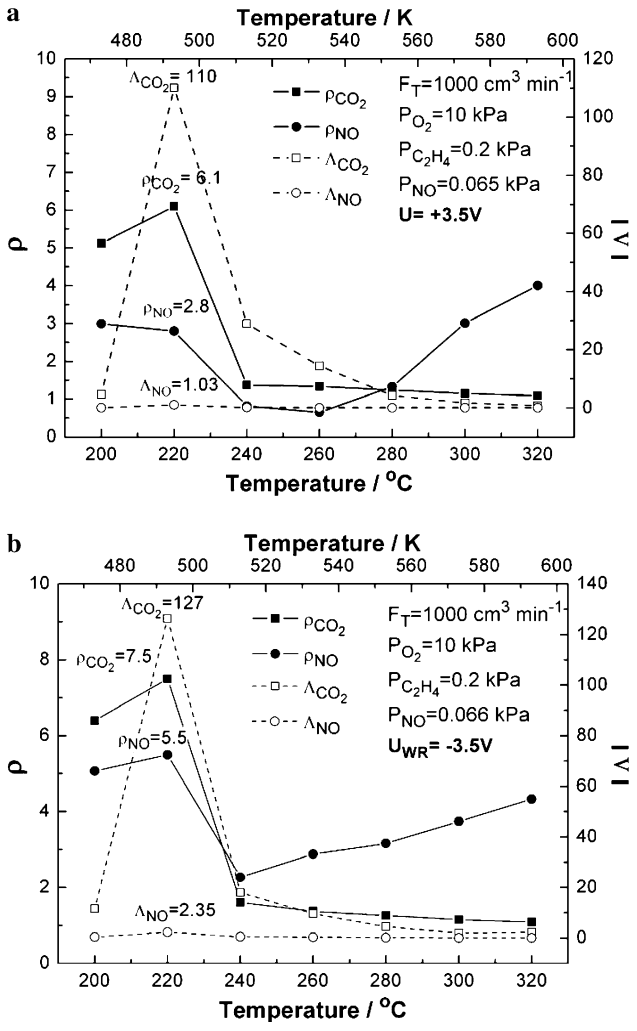

Fig. 9 Steady state effect of temperature on the rate enhancement ratio (ρ) and Faradaic efficiency (Λ) for both CO_2 formation and NO conversion under both positive (**a**) and negative (**b**) potential imposition under highly oxidizing conditions

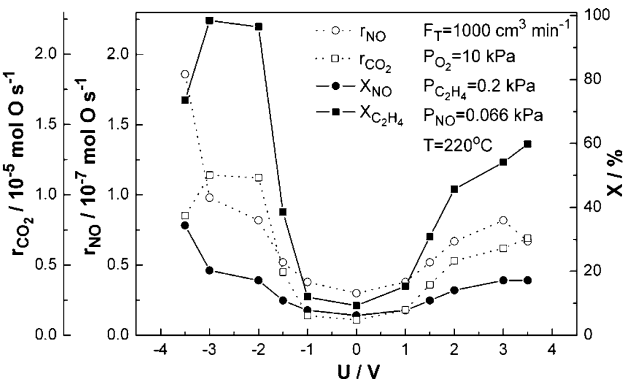

Fig. 10 Steady state effect of the applied potential on the NO conversion rate (r_{NO}), on the CO_2 formation rate (r_{CO_2}) and on the conversion of NO and C_2H_4 (X_{NO}, $X_{C_2H_4}$) at T = 220 °C, and highly oxidizing conditions

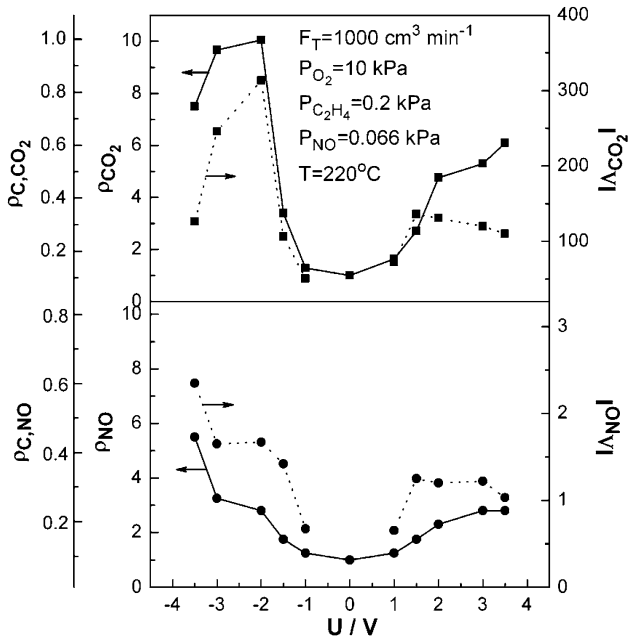

Fig. 11 Steady state effect of the applied potential on the rate enhancement ratio (ρ), on the effective enhancement ratio (ρ_c) and on the apparent Faradaic efficiency (Λ) for CO_2 formation and NO conversion at T = 220 °C, and highly oxidizing conditions

4 Conclusions

The present results appear to be of significant practical usefulness for the development of efficient commercial catalytic converters for lean burn or Diesel engines. In relation to previous exploratory studies of electrochemical promotion using Rh/YSZ/Pt elements and monolithic electropromoted reactors [34–36], the present study has identified optimal performance at low temperatures (220–240 °C) and pronounced electropromotion even under highly oxidizing conditions ($\lambda = 16.7$). In this narrow temperature range the selectivity to N_2 obtained with the Rh/YSZ/Pt elements is near 100% and the production of CO, N_2O and NO_2 is almost undetectable. This significant enhancement in performance may be to a small extent due to the reactor gas-tightness improvement, but is primarily due to the significantly lower (220 °C) operating temperatures studied in the present investigation. It will be interesting to test more such units operating at 220−240 °C in the exhaust of Diesel engines [37] in order to examine long term performance and stability.

Acknowledgements We thank the AKMON programme of the General Secretariat for research and development (GSRT) for partial financial support and our reviewers for helpful comments.

Appendix 1 Studies of the electrochemical promotion of NO reduction until 10/2007 (Refs. [24–49])

Electrolyte	Electrode	Temperature (°C)	Lean/rich	Rate enhancement (max)	Selectivity to N_2	Refs.
YSZ	Ir	200–500	C_3H_6=NO = 0.2 kPa O_2 = 1 and 5 kPa	O_2 = 1 kPa: yield N_2 unpromoted 38%, promoted 64%	Yield N_2O ~7% unpromoted and promoted	[24]
YSZ	Pd	320–480	CO = 0.5 kPa NO = 0.75 kPa No O_2	$\rho N_2 = 2.6$	Unpromoted 33%, promoted 47%	[25]
YSZ	Pd	373	CO = 0.55 kPa NO = 1.34 kPa No O_2	$\rho N_2 = 3.1$ $\rho N_20 = 1.5$	Unpromoted 22%, promoted 35%	[26]
YSZ	Pd	370	CO = 0.65 kPa NO = 0.61 kPa	$\rho N_2 = 4.2$ $\rho N_20 = 2.2$ $\rho CO_2 = 2.2$		[27]
YSZ	Pt	230–410	C_3H_6=NO = 0.2 kPa O_2 = 1 kPa	$\rho N_2 = 1.9$	Unchanged	[28]
YSZ	Rh	300	C_3H_6:NO = 1 kPa O_2 = 0.5 kPa	$\rho N_2 = 3$	Unpromoted/ promoted 50%	[29]
YSZ	Rh	250–400	CO = 0.3 kPa NO = 0.1 kPa O_2 = 0.85–1.4 kPa	$\rho N_2 = 10$ $\rho N_20 = 3$	Below 350°C 5% Above 420°C 20%	[30]
YSZ	Rh	250–430	C_3H_6 = 0.085 kPa NO = 0.07 kPa O_2 = 0.3 and 2 kPa	380°C: $\rho N_2 = 10$, $\rho N_2O = 3$ 430°C: $\rho N_2 = 49$	T = 430°C no N_2O	[31]

Appendix 1 continued

Electrolyte	Electrode	Temperature (°C)	Lean/rich	Rate enhancement (max)	Selectivity to N_2	Refs.
YSZ	Rh	430	C_3H_6 = 0.85 kPa NO = 0.7 kPa O_2 0.3 and 2 kPa	ρN_2 = 3–11	100%	[30]
YSZ	Rh	320–440	CO = 0.3 kPa NO = 0.1 kPa O_2 = 0.3–2 kPa	ρN_2 = 10 ρN_20 = 3	Below 350°C 50% Above 420°C 100%	[32]
YSZ	Rh–Ag (7:1)	386	C_3H_6:NO = 0.1 kPa O_2 = 5 kPa	ρN_2 = 8 ρN_2O = 3	Unpromoted 28%, promoted 55%	[33]
YSZ/Pt MEPR 21 plate operation	Rh	300–330	C_2H_4 = 0.36 kPa NO = 0.14 kPa O_2 = 1.1 kPa	T = 320°C ρNO = 1.33 Conversion unpromoted 60% Promoted 80%	Not given	[34]
YSZ/Au MEPR 11 plate operation	Rh	305	C_2H_4 = 0.36 kPa NO = 0.11 kPa O_2 = 1.1 kPa	ρNO = 1.8 Conversion unpromoted 30.5% Promoted 56%	Not given	[35]
YSZ/Au MEPR 11 plate operation	Rh	305	C_2H_4 = 0.36 kPa NO = 0.11 kPa O_2 = 1.1 kPa	ρNO = 1.8 Conversion unpromoted 30.5% Promoted 56%	Not given	[36]
YSZ/Pt MEPR	Rh	290–330	Real engine exhaust gas test NO = 0.037 kPa CO_2 = 8.3 kPa O_2 = 9.8 kPa Fuel = 0.23 kPa	ρNO < 1 NO_x conversion unpromoted < 5 promoted 30%	Not given	[37]
YSZ/Au MEPR	Rh:Pt	335–380	NO = 0.065 kPa C_2H_4 = 0.2 kPa O_2 = 0.8–10 kPa	O_2 = 0.8 kPa ρNO = 2.32 O_2 = 10 kPa ρNO = 1.26	N_2O and NO_2 not detected	[38]
YSZ	Rh	370	C_3H_6=NO = 0.1 kPa O_2 = 0.3–4.8 kPa	ρN_2 = 55 ρCO_2 = 220	$O_2 \leq$ 2.5 kPa 100% O_2 > 2.5 kPa significant NO_2 formation	[39]
β''-Al_2O_3 K^+ promoted	Ir	250–400	C_3H_6=NO = 0.2 kPa O_2 = 0–5 kPa	Poisoning of K^+ for CO_2 and N_2 formation rate at all O_2 < 0 kPa	60–100%	[40]
β''-Al_2O_3	Pt	280–400	CO = NO = 3:1 No O_2	Not given	Not given	[41]
β''-Al_2O_3	Pt	320–400	CO:NO = 0.75 kPa No O_2	ρN_2 = 13 ρN_20 = 1.5	Unpromoted 15%, promoted 65%	[42]
β''-Al_2O_3	Pt	300–430	NO = 0–1.6 kPa H_2 = 0–1 kPa No O_2	ρN_2 = 18 ρN_20 = 11	Unpromoted 35%, promoted 70%	[43]

Appendix 1 continued

Electrolyte	Electrode	Temperature (°C)	Lean/rich	Rate enhancement (max)	Selectivity to N_2	Refs.
β''-Al_2O_3	Pt	361	C_3H_6 = 0–0.6 kPa NO = 1.3 kPa No O_2	$\rho N_2 = 20$	Unpromoted 60%, promoted 80%	[44]
β''-Al_2O_3	Pt		C_3H_6=NO = 0.2 kPa	T = 220°C ρNO < 1.5	T < 340°C N_2O	[45]
Na^+ promoted			O_2 = 0.5–5 kPa	T > 220°C poisson	T > 300°C NO_2	
β''-Al_2O_3	Pt	240	C_3H_6=NO = 0.2 kPa	O_2 = 0.5 kPa: ρNO = 1.4	O_2 = 0.5 and 1 kPa: $S_{N2} > 50\%$	[46]
Na^+ promoted			O_2 = 0.5–5 kPa	O_2 = 5 kPa: ρNO = 1	O_2 = 5 kPa: $S_{N2} < 45\%$	
β''-Al_2O_3	Rh	310	CO:NO = 1 kPa		Unpromoted 23%, promoted 75%	[47]
	Cu	310	No O_2 CO = 2 kPa NO = 1 kPa No O_2		Unpromoted < 5%, promoted 95%	
β''-Al_2O_3	Rh	322	CO:NO = 0.9 kPa O_2 = 0–2 kPa	O_2 = 0: $\rho N_2 = 1.5$, $\rho N_2O = 0.38$ O_2 = 2: $\rho N_2 = 1$, $\rho N_2O = 1$	O_2 = 0: unpromoted 54%, promoted 82% O_2 = 2: unpromoted/ promoted 24%	[48]
β''-Al_2O_3	Rh	350	C_3H_6:NO = 0.1 kPa O_2 = 0–2 kPa	O_2 = 0: $\rho N_2 = 1.89$, $\rho N_2O = 0.47$ O_2 = 2: $\rho N_2 = 0.07$, $\rho N_2O = 0.1$	O_2 = 0: unpromoted 49%, promoted 78% O_2 = 2: unpromoted 55% promoted 52%	[48]
β''-Al_2O_3	Rh	307	CO:NO = 1 kPa No O_2	$\rho N_2 = 3.1$ $\rho N_2O = 0.3$	Unpromoted 24%, promoted 80%	[49]
β''-Al_2O_3	Rh	350	C_3H_6:NO = 1 kPa No O_2	$\rho N_2 = 2.4$ $\rho N_2O = 0.4$	Unpromoted 45%, promoted 82%	[49]
Nasicon	Pt	200–400	C_3H_6=NO = 0.2 kPa O_2 = 5 kPa	$\rho N_2 = 1.7$ $\rho N_2O = 1.5$	Anodic polarization: Unpromoted 41% Promoted 61% Cathodic polarization: Unpromoted 41% Promoted 73%	[50]
Proton conductor	Pt	100–350	N0 = 800 ppm H_2 = 0–8400 ppm O_2 = 0–10 kPa			[51]

References

1. Burch R, Watling TC (1997) Appl Catal B 11207:216
2. Obuchi A, Kaneko I, Oi J, Ohi A, Ogata A, Bamwenda GR, Kushiyama S (1998) Appl Catal B 15:37
3. Amiridis MD, Zhang T, Farrauto RJ (1996) Appl Catal B 10:203
4. Pavulescu VI, Grange P, Delmon B (1998) Catal Today 46:233
5. Fritz A, Pitchon V (1997) Appl Catal B 13:1
6. Halkides TI, Kondarides DI, Verykios XE (2002) Catal Today 73:213
7. Kotsifa A, Halkides TI, Kondarides DI, Verykios XE (2002) Catal Lett 79:113
8. Čapek L, Dědeček J, Wichterlová B, Cider L, Jobson E, Tokarová V (2005) Appl Catal B 60:147
9. Čapek L, Novoveska K, Sobalik Z, Wichterlová B, Cider L, Jobson E (2005) Appl Catal B 60:201
10. Nikopoulos AA, Stergioula ES, Efthimiadis EA, Vasalos IA (1999) Catal Today 54:439
11. Vernoux P, Leinekugel-Le-Cocq AY, Gaillard F (2003) J Catal 219:247
12. Yentekakis I, Tellou V, Botzolaki G, Rapakousios I (2005) Appl Catal B 56:229
13. Joubert E, Courtois X, Marecot P, Canaff C, Duprez D (2006) J Catal 243:252
14. Chen LF, Gonzalez G, Wang JA, Norena LE, Toledo A, Castillo S, Moran-Pineda M (2005) Appl Surf Sci 243:319
15. Wang X, Xu Y, Yu S, Yang C (2005) Catal Lett 103:101

16. Lintz HG, Vayenas CG (1989) Angew Chem Int Ed Engl 28(6):708
17. Vayenas CG, Bebelis S, Neophytides S, Yentekakis IV (1989) Appl Phys A 49:95
18. Stoukides M, Vayenas CG (1981) J Catal 70:137
19. Vayenas CG, Bebelis S, Ladas S (1990) Nature 343:625
20. Lambert RM, Williams F, Palermo A, Tikhov MS (2000) Top Catal 13:91
21. Foti G, Wodiunig S, Comninellis C (2000) Curr Top Electrochem 7:1
22. Cavalca CA, Haller GL (1998) J Catal 177:389
23. Vayenas CG, Bebelis S, Pliangos C, Brosda S, Tsiplakides D (2001) In: Electrochemical activation of catalysis: promotion, electrochemical promotion and metal–support interactions. Kluwer Academic/Plenum Publishers, New York, references therein
24. Vernoux P, Gaillard F, Karoum R, Billard A (2007) Appl Catal B 73:73
25. Marwood M, Kaloyannis A, Vayenas CG (1996) Ionics 2:302
26. Marwood M, Vayenas CG (1997) J Catal 170:275
27. Kim S, Haller GH (2000) Solid State Ionics 136(137):693
28. Beguin B, Gaillard F, Primet M, Vernoux P, Bultel L, Henault M, Roux C, Siebert E (2002) Ionics 8:128
29. Foti G, Lavanchy O, Comninellis Ch (2000) J Appl Electrochem 30:1223
30. Pliangos C, Raptis C, Badas Th, Vayenas CG (2000) Ionics 6:119
31. Pliangos C, Raptis C, Badas Th, Vayenas CG (2000) Solid State Ionics 136(137):767
32. Pliangos C, Raptis C, Badas Th, Tsiplakides D, Vayenas CG (2000) Electrochim Acta 46:331
33. Williams FJ, Macleod N, Tikhov MS, Lambert RM (2002) Electrochim Acta 47:1259
34. Balomenou SP, Tsiplakides D, Katsaounis A, Thiemann-Handler S, Cramer B, Foti G, Comninellis Ch, Vayenas CG (2004) Appl Catal B 52:181
35. Tsiplakides D, Balomenou S, Katsaounis A, Archonta D, Koutsodontis C, Vayenas CG (2005) Catal Today 100:133
36. Balomenou SP, Tsiplakides D, Katsaounis A, Brosda S, Hammad A, Foti G, Comninellis Ch, Thiemann-Handler S, Cramer B, Vayenas CG (2006) Solid State Ionics 171:2201
37. Balomenou S, Tsiplakides D, Vayenas CG, Poulston S, Houel V, Collier P, Konstandopoulos A, Agrafiotis Ch (2007) Top Catal 44(3):481
38. Koutsodontis C, Hammad A, Lepage M, Sakamoto Y, Fóti G, Vayenas CG (2008) Top Catal (in press)
39. Constantinou I, Archonta D, Brosda S, Lepage M, Sakamoto Y, Vayenas CG (2007) J Catal 251:400
40. Goula G, Katzourakis P, Vakakis N, Papadam T, Konsolakis M, Tikhov M, Yentekakis IV (2007) Catal Today 127:199
41. Harkness IR, Lambert RM (1995) J Catal 152:211
42. Palermo A, Lambert RM, Harkness IR, Yentekakis I, Marina O, Vayenas CG (1996) J Catal 161:471
43. Marina OA, Yentekakis IV, Vayenas CG, Palermo A, Lambert RM (1997) J Catal 166:218
44. Yentekakis IV, Palermo A, Filkin NC, Tikhov MS, Lambert RM (1997) J Phys Chem B 101:3759
45. Dorado F, de Lucas-Consuegra A, Jimenez C, Valverde JL (2007) Appl Catal A 321:86
46. Dorado F, de Lucas-Consuegra A, Vernoux P, Valverde JL (2007) Appl Catal B 73:42
47. Lambert RM, Palermo A, Williams FJ, Tikhov MS (2000) Solid State Ionics 136(137):677
48. Williams FJ, Tikhov MS, Palermo A, Maclead N, Lambert RM (2001) J Phys Chem B 105:2800
49. Williams FJ, Palermo A, Tikhov MS, Lambert RM (2001) Surf Sci 482(485):177
50. Vernoux P, Gaillard F, Lopez C, Siebert E (2003) J Catal 217:203
51. Tomita A, Yoshii T, Teranishi S, Nagao M, Hibino T (2007) J Catal 247:137